mental growth as described in (*21*). Resolution decreased with ontogeny because of diminished increment width with age. $\delta^{18}\rightarrow \delta^{18}O_{otolith}$ ratios are reported relative to Pee Dee belemnite (PDB) standard, and water oxygen isotope ratios are reported relative to Standard Mean Ocean Water (SMOW) using conventional per mil (‰) notation. Precision of isotope analyses is as follows: conventional H_3PO_4 extraction (of aragonite) is ± 0.1‰ (1σ), laser ablation extraction (of aragonite) is ±0.2‰ (1σ), and CO_2 equilibration (of water) is ± 0.1‰ (1σ). Precision was calculated based on between- and within-run comparisons of working standards.

22. SST data from the Joint Institute for the Study of the Atmosphere and the Oceans database can be found online at http://tao.atmos.washington.edu/data_sets/for Puerto Chicama (8°S, 1989–1999) and Paita (5°S, 1989–1998), and measured $\delta^{18}O_{water}$ values (–0.5 ± 0.2‰ 1σ; n = 4) were applied to the aragonite $\delta^{18}O$ temperature equation (*24*) to build models of $\delta^{18}O_{otolith}$ profiles.
23. Figure 3A compares model $\delta^{18}O_{otolith}$ values to the composite mean $\delta^{18}O$ of 10 modern otoliths. The composite was constructed by calculating the mean $\delta^{18}O$ value of each increment in every otolith. These values were averaged with all other contemporaneous increments to produce the 6-month time-average composite. The mean $\delta^{18}O$ of the modern otoliths is –0.1‰ (1σ = 0.4), with a mean seasonal $\delta^{18}O$ range of 1‰ (1σ = 0.3). Modeled and measured isotope profiles were strongly correlated, thus documenting $\delta^{18}O_{otolith}$ records as valid proxies for SSTs.
24. E. L. Grossman, T. L. Ku, *Chem. Geol.* **59**, 59 (1986).
25. S. Pozorski, T. Pozorski, *Ann. Carnegie Mus.* **48**, 337 (1979).
26. ———, *J. Field Archaeol.* **13**, 381 (1986).
27. E. J. Reitz, unpublished data.
28. C. E. Shannon, W. Weaver, *The Mathematical Theory of Communication* (Univ. of Illinois Press, Urbana, IL, 1949).
29. S. H. Hurlbert, *Ecology* **52**, 577 (1971).
30. D. Pauly, V. Christensen, *Nature* **374**, 255 (1995).
31. R. Froese, D. Pauly, *Fishbase*, online at www.fishbase.org (2 March, 2001).
32. Diversity was calculated by $H' = \sum_{i=1}^{S}(p_i)(\log p_i)$, where H' = diversity, $\sum_{i=1}^{S}$ = the sum of all taxa, and p_i = relative abundance of i^{th} taxon (*28*). Equitability was calculated by $V' = H'/\log S$, where V' = equitability and S = number of taxa (*29*). Trophic level determination was based on data in (*31*), or the nearest approximation based on analog species. Trophic value was determined for each taxon identified and multiplied by its MNI, and then the total of all trophic values was divided by total-site MNI. All sites were excavated in a similar fashion, and we used fine mesh-screen recovery, thus minimizing recovery bias and ensuring representative samples.
33. D. H. Sandweiss, K. A. Maasch, D. F. Belknap, J. B. Richardson III, H. B. Rollins, *J. Coastal Res.* **14**, 367 (1998).
34. C. Perrier, C. Hillaire-Marcel, L. Ortlieb, *Geogr. Phys. Quat.* **48**, 23 (1994).

35. We thank B. McClain for assistance with isotopic analysis and M. Cornejo for field assistance. Funded in part by grants from the Geological Society of America (C.F.T.A.), Explorer's Club International (C.F.T.A.), NSF grant ATM-0082213 (D.E.C.), The Heinz Charitable Trust (D.H.S.), the University of Maine Faculty Research Fund (D.H.S.), and Department of Energy grant DE-FC09-96SR18546 (C.S.R.).

26 April 2001; accepted 14 January 2002

Abrupt Decrease in Tropical Pacific Sea Surface Salinity at End of Little Ice Age

Erica J. Hendy,[1]* Michael K. Gagan,[1] Chantal A. Alibert,[1] Malcolm T. McCulloch,[1] Janice M. Lough,[2] Peter J. Isdale[2]

A 420-year history of strontium/calcium, uranium/calcium, and oxygen isotope ratios in eight coral cores from the Great Barrier Reef, Australia, indicates that sea surface temperature and salinity were higher in the 18th century than in the 20th century. An abrupt freshening after 1870 occurred simultaneously throughout the southwestern Pacific, coinciding with cooling tropical temperatures. Higher salinities between 1565 and 1870 are best explained by a combination of advection and wind-induced evaporation resulting from a strong latitudinal temperature gradient and intensified circulation. The global Little Ice Age glacial expansion may have been driven, in part, by greater poleward transport of water vapor from the tropical Pacific.

The Little Ice Age (LIA) appears in most Northern Hemisphere paleoclimate reconstructions as multiple, century-scale periods of anomalously cold, dry conditions between the 15th and late 19th centuries (*1–4*). Glacial advances in both hemispheres (*1*) and enhanced polar atmospheric circulation (*5*) suggest that the LIA was a global-scale event. With the exception of the Quelccaya ice core record from equatorial Peru (*6*), however, the sparse reconstructions of the LIA available from the tropics and Southern Hemisphere fail to identify synchronous cold periods (*7, 8*). An alternative scenario is that cooling during the LIA was restricted to higher latitudes (*9, 10*). We examine the nature of the LIA in the tropical southwestern Pacific since 1565 using coral proxies to reconstruct sea surface temperature (SST) and salinity (SSS), the key indicators of climate change within the tropical ocean-atmosphere system.

We present 420-year records of three coral paleoclimate tracers, $\delta^{18}O$, Sr/Ca, and U/Ca, constructed from replicated measurements of eight cores from massive *Porites* sp. colonies (Fig. 1). The cores were collected at seven reefs, 12 to 120 km apart, from the central Great Barrier Reef (GBR), Australia [for details and site maps, see (*11*)]. The use of multiple cores allows us to test the fidelity of individual tracers over century time scales and to establish regional-scale proxy climate signals. Coral $\delta^{18}O$, the most frequently used coral climate proxy tool, reflects a combination of SST and the seawater $\delta^{18}O$ composition. The latter responds to changes in SSS caused by shifts in seawater $\delta^{18}O$ produced by evaporation and freshwater input. By using parallel measurements of the coral paleothermometers Sr/Ca and U/Ca to determine SST, we are able to separate SST variation from changes in seawater $\delta^{18}O$ (*12, 13*). This approach allows us to resolve both SST and SSS over the past four centuries.

Five-year bulk increments were sampled for equivalent periods across all eight cores after cross-dating with ultraviolet (UV) fluorescent bands; x-radiography was used to reveal annual density banding (*14*). Fine powder was milled from 2-mm square-section grooves along the center of the coral growth axis, homogenized, and subsampled for stable isotope and trace element analysis (*15*). Figure 1 shows the replicated measurements combined into a composite record, with the variability between corals shown as a 95% confidence envelope calculated for each pentannual interval (*16*). Individual $\delta^{18}O$ records reproduce not only the century-scale trends in the composite $\delta^{18}O$ reconstruction but also decadal variations of up to 0.26‰, capturing on average 72% of the shared $\delta^{18}O$ signal. Intercoral variability is greater between individual Sr/Ca and U/Ca records, which share on average 33% and 26%, respectively, of the common variance. When converted to temperature by applying accepted SST-slope calibrations (*17, 18*), the Sr/Ca record is better constrained than the U/Ca record (Sr/Ca, ±0.3°C; U/Ca, ±0.5°C). This intercoral Sr/Ca variability is equivalent to that found between high-resolution seasonal records from *Porites* colonies at sites close to those used here (*13, 17*). However, multiple Sr/Ca or U/Ca records are required to reconstruct decadal to century-scale SST signals, which in the GBR are one-tenth the size of seasonal variations.

The Sr/Ca and U/Ca composite records, converted to SST anomalies (SSTA), are verified against GISST2.2 (*19*) for the 1° grid at 18°S, 146°E (resampled to 5-year averages, 1905 to 1985). Linear regressions are signif-

[1]Research School of Earth Sciences, Australian National University, Canberra, ACT 0200, Australia. [2]Australian Institute of Marine Science, PMB 3, Townsville M.C., Queensland 4810, Australia.

*To whom correspondence should be addressed. E-mail: erica.hendy@anu.edu.au

icant at the 99% level for both Sr/Ca (r = 0.68) and U/Ca (r = 0.63). The Sr/Ca and U/Ca SSTA reconstructions are in excellent agreement (r = 0.72, $P < 0.001$, n = 81). Although the temperature calibrations (*17, 18*) were developed from short high-resolution records, both reconstructions successfully reproduce the 0.7°C warming evident over the 80-year GISST2.2 series (Sr/Ca, +0.7°C; U/Ca, +1.0°C). Furthermore, the coral paleotemperature reconstructions compare reasonably well with the U.K. Meteorological Office tropical western Pacific SSTA composite record for 1865 to 1985 [20°N to 20°S, 120°E to 170°W (*20*)], despite significant uncertainty in the instrumental record before ~1900 (Sr/Ca, r = 0.58; U/Ca, r = 0.58; $P < 0.005$) (Fig. 2, A to C). This indicates that the coral SSTA reconstructions from the GBR are regionally significant.

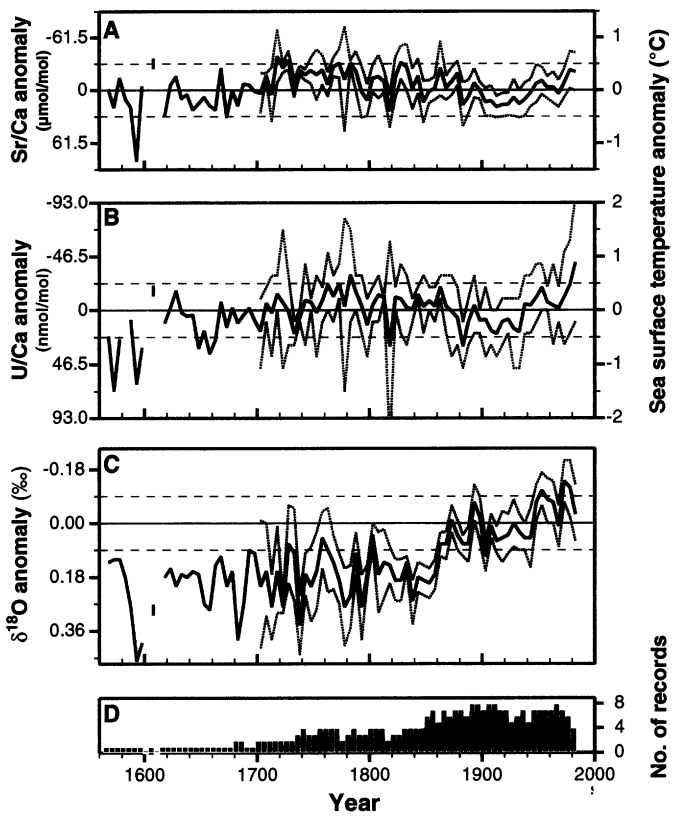

Fig. 1. GBR composite records of **(A)** Sr/Ca, **(B)** U/Ca, and **(C)** $\delta^{18}O$ at pentannual resolution. Solid lines show the average reconstruction (*16*) normalized to the period 1860 to 1985, plotted as ratios (left axis) and SSTA (right axis). The 95% confidence intervals are shown by the dotted lines surrounding the solid line of the reconstruction. SSTA conversions are −61.5 μmol/mol per °C for Sr/Ca (*17*) and −46.5 nmol/mol per °C for U/Ca (*18*). The horizontal dashed lines define a 1°C band according to these slope calibrations. **(D)** The number of records averaged at each pentannual interval for the $\delta^{18}O$ reconstruction.

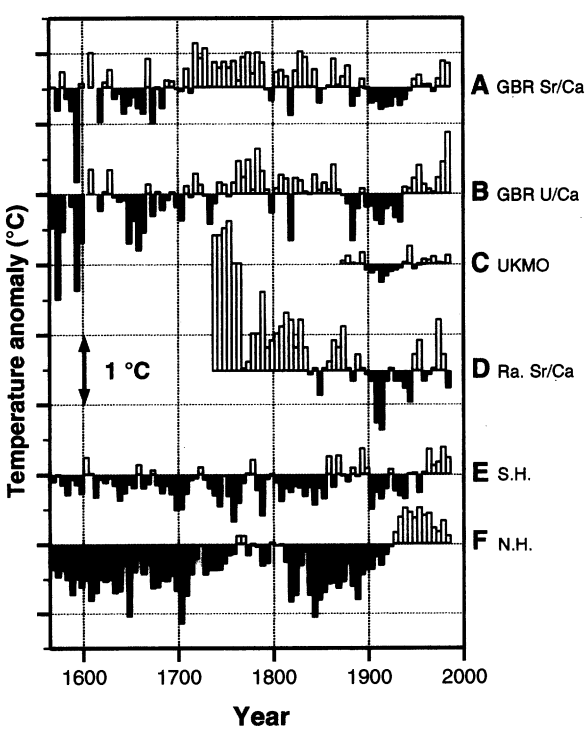

Fig. 2. A comparison of coral and instrumental temperature records. GBR composite SSTA reconstructions were derived from coral Sr/Ca **(A)** and U/Ca **(B)** and were converted to SSTA using slope calibrations from (*17*) and (*18*), respectively. **(C)** UKMO composite SSTA records for the tropical western Pacific [20°N to 20°S, 120°E to 170°W (*20*)]. **(D)** The Rarotonga Sr/Ca SST record (21.5°S, 159.5°W) of Linsley *et al.* (*21*) is plotted using the Sr/Ca SST slope calibration given in (*21*). **(E** and **F)** Proxy temperature (land and SST) compilations for the Southern and Northern Hemispheres, respectively (*7*). Jones *et al.* (*7*) cautioned that the Southern Hemisphere reconstruction (E) is a poor representative of temperature because it is constructed from only seven paleotemperature records. All records plotted for comparison are resampled to equivalent 5-year averages, and all series are normalized to the common period 1860 to 1985.

The Sr/Ca and U/Ca records reconstruct SSTs that were ~0.2° to 0.3°C cooler than the long-term average during an extended period from 1565 to 1700 (Fig. 2, A and B). After a century-scale warming of 0.4°C centered on 1700, above-average SSTs persist through most of the 18th and 19th centuries before cooling to a minimum in the early 20th century. From this cold interval, the SSTA reconstructions capture the 20th century warming until the 1980s, when the coral cores were collected. It is conspicuous that the period from the 1700s to the 1870s was consistently as warm as the early 1980s. The only other Pacific coral Sr/Ca record, from Rarotonga (Fig. 2D) (*21*), also reconstructs SSTs for the 18th and 19th centuries that are as warm as, or warmer than, the 20th century.

The question raised by our coral SSTA reconstructions is whether the positive temperature anomalies during the LIA were limited to the tropical Pacific (or to the tropics as a whole) or penetrated throughout the Southern Hemisphere. The small number of proxy temperature records from the Southern Hemisphere, and their conflicting signals, limit attempts to describe regional patterns (*4, 7, 8*) (Fig. 2, E and F). In contrast, global proxy temperature composites consistently show that the 20th century was significantly warmer than the four preceding centuries (*7, 22–24*). Available proxy sources, however, are predominantly land-based and from the temperate Northern Hemisphere, and therefore are unlikely to be representative of the global-scale response. The recovery to warmer conditions seen in the global and hemispheric composites coincides with the glacial retreat that signaled the end of the LIA in the late 19th to early 20th centuries (*1*), while at the same time, the tropical Pacific cooled according to our coral SSTA reconstructions. If the LIA cooling was limited to higher latitudes, then latitudinal SST gradients were greater than at present, in turn intensifying the poleward transport of heat in the atmosphere and ocean (*9, 10*). Evaporation and condensation are effective processes for redistributing atmospheric heat between the tropics and extratropics. Measurements of coral $\delta^{18}O$ enable us to monitor changes in the tropical hydrological balance through the isotopic change in seawater as it is enriched in ^{18}O by evaporation and depleted in ^{18}O by freshwater input (*25*).

The most striking feature of the composite 420-year $\delta^{18}O$ GBR coral record is the abrupt

0.2‰ shift between 1850 and 1870 toward lower modern $\delta^{18}O$ values (Fig. 3A). Superimposed on this century-scale signal are interdecadal $\delta^{18}O$ cycles of up to 0.26‰. Only a very weak relationship is seen between the coral $\delta^{18}O$ and paleotemperature proxies. By taking into account the SST anomalies recorded by the coral Sr/Ca, we are able to subtract the component of $\delta^{18}O$ related to temperature and to resolve the salinity effect from the residual (*26*). The residual $\delta^{18}O$ (Fig. 3B) shares more than 80% of its variance with the original $\delta^{18}O$ reconstruction, indicating that the long-term ^{18}O depletion since the 1870s was the result of a significant freshening of the GBR lagoon waters in the modern period. This late-19th century shift is recorded synchronously by $\delta^{18}O$ coral records throughout the Coral Sea (Fig. 3), including Abraham Reef on the southern outer edge of the GBR (*27*), New Caledonia (*28*), and Espirtu Santos, Vanuatu (*29*). Supporting a southwestern Pacific–wide SSS-dominated $\delta^{18}O$ signal is the lack of any relationship between instrumental SST and either the Vanuatu or Abraham Reef $\delta^{18}O$ records (*30*). It has also been proposed that salinity is more influential at frequencies lower than interannual periods in the New Caledonia coral $\delta^{18}O$ signal (*31*). These results suggest that, in addition to warm SSTs, conditions in the tropical southwestern Pacific during the LIA were also consistently more saline.

Reduced precipitation during the LIA, associated with a change in the position of the Intertropical Convergence Zone, was suggested to explain a similar century-scale $\delta^{18}O$ shift around 1850 seen in the Gulf of Chiriquí $\delta^{18}O$ coral record in the Eastern Pacific (*32*). The strength of the Australian summer monsoon influences SSS in the GBR (*33*) and is an important source of the interdecadal coral $\delta^{18}O$ variability [$r = 0.74$ for $\Delta\delta^{18}O$ and Queensland summer rainfall index 1890–1985 (*34*)]. However, as explained below, three centuries of drier conditions cannot alone account for the $\delta^{18}O$ enrichment in the GBR corals before 1870. Twenty-six percent of the land area of Queensland drains into the GBR, and discharge records from the largest freshwater contributor, the Burdekin River, also correlate strongly with coral $\delta^{18}O$ [$r = 0.70$, 1895–1985 (*35*)]. Extrapolation of this relationship would imply that the river ceased flowing for most of the period from 1565 to 1860. Such an extreme hydrological reconstruction is contradicted by coral UV fluorescence records, which are excellent recorders of regional river discharge to the GBR and provide an independent estimate of Queensland's precipitation (*35*). Fluorescence records indicate that river flow into the GBR continued throughout the last four centuries (*14, 35*). In addition, a multicentury drought should dampen coral $\delta^{18}O$ variability; instead, the amplitude of interdecadal oscillations is greatest during the 18th century. Finally, the $\delta^{18}O$ depletion after ~1870 is common to each of the southwestern Pacific coral sites despite their different rainfall regimes, proximities to terrestrial sources, and land-use histories.

Additional processes that influence seawater $\delta^{18}O$ uniformly throughout the southwestern Pacific must be implicated in the 1870s century-scale $\delta^{18}O$ shift. Both surface-ocean evaporation and advection are also important factors modifying SSS in the Coral Sea (*36*), and their contribution to the $\delta^{18}O$ shift is supported by paleo-evidence for weakened trade winds and altered oceanic circulation since the mid-19th century. Globally, one of the most consistent features identified in historical and paleoclimate records of the LIA is enhanced and highly variable atmospheric circulation (*1–3, 5*). Large-scale changes in tropical atmospheric circulation are clearly evident in the Peruvian Quelccaya ice core [14°S, 71°W (*6*)], which provides a high-resolution aeolian record of the Southern Hemisphere trade wind belt (Fig. 3G). Greater dust deposition in the ice cap is indicative of increased wind velocities across the altiplano of Southern Peru (*6*). During the LIA the number of large aeolian particles (diameter >1.59 μm) increased relative to the rest of the ice core, along with abrupt 20% to 30% shifts in microparticles and conductivities (*6*). Significant correlations between the Quelccaya large particle concentrations and $\delta^{18}O$ coral records from the southwestern Pacific ($r = 0.57$ for GBR coral $\delta^{18}O$) highlight the potential for intensified atmospheric circulation to affect both regions.

We propose that during the LIA, strengthened trade winds influenced the southwestern Pacific evaporation-precipitation balance by enhancing regional evaporation, causing the seawater and coral to be enriched in ^{18}O. A change of trade wind influence in the southwestern Pacific is also evident in the varying strength of the western boundary current. The South Equatorial Current (SEC) transports characteristically high salinity (~35.6 psu) water westward into the Coral Sea before branching south along the GBR as the East Australian Current (*37*). Coral $\Delta^{14}C$ records from Abraham Reef (*27*) and Heron Island, GBR (*38*) are consistent with the scenario of a weakening of these currents as

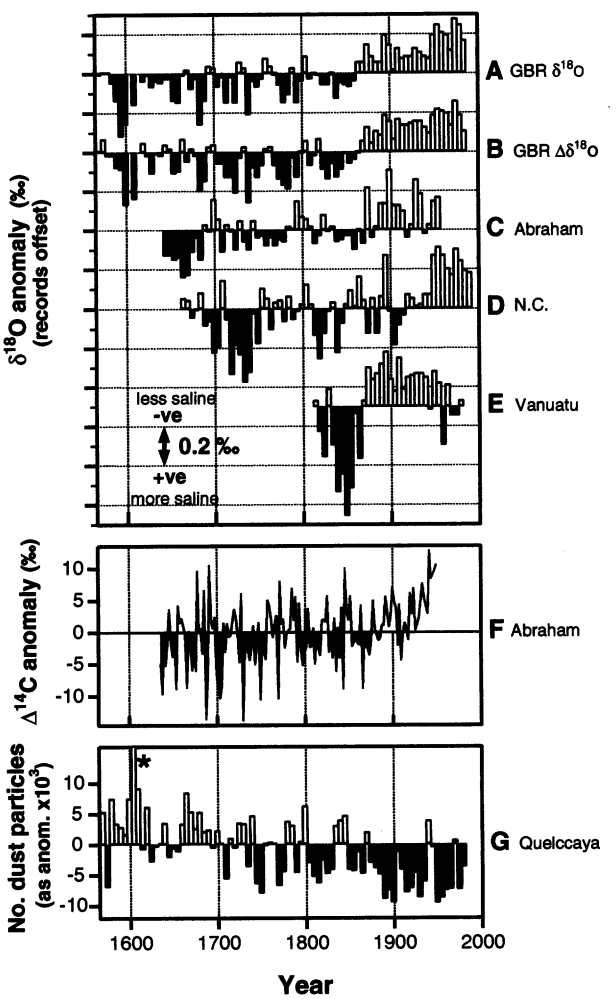

Fig. 3. Comparison of regional coral $\delta^{18}O$ records and proxies of Southern Hemisphere ocean-atmosphere circulation. The composite GBR $\delta^{18}O$ record (**A**) is reduced to a residual $\delta^{18}O$ record (**B**) by subtracting the temperature signal from the GBR Sr/Ca record. Propagation of total uncertainties gives an average 95% confidence interval for (B) of ±0.15‰ from 1700 to 1780 and ±0.11‰ from 1780 to 1985. The three southwestern Pacific $\delta^{18}O$ records are (**C**) Abraham Reef, GBR (22°S, 153°E) (*27*), (**D**) Amedée Lighthouse, New Caledonia (22°S, 166°E) (*28*), and (**E**) Espirtu Santos, Vanuatu (15°S, 167°E) (*29*). All records are resampled to equivalent 5-year averages, and each $\delta^{18}O$ record is normalized to the average of the whole record. (**F**) The annual Abraham Reef $\Delta^{14}C$ record of Druffel and Griffin (*27*) is calculated as an anomaly relative to the expected ocean mixed-layer estimates of $\Delta^{14}C$ [values reported by (*27*) in Fig. 1B]. The $\Delta^{14}C$ estimates were modeled from 20-year tree-ring (atmospheric) $\Delta^{14}C$ values and an ocean box-diffusion model (*39*). (**G**) Number of large particles (diameter >1.59 μm) in the Quelccaya ice core (14°S, 71°W) (*6*) plotted as an anomaly from the mean (1560 to 1980). The asterisk highlights the extreme dust concentrations corresponding to the local eruption of Huaynaputina, Peru, in 1600 (*6*).

a result of lower wind stress since the LIA. The absence of the "Suess effect" (the lowering of $\Delta^{14}C$ values from the late 19th century as fossil fuel burning released ^{14}C-free CO_2) in these records is interpreted as a long-term change in ocean circulation within the southwestern Pacific since the late 1800s (*38*). Rising $\Delta^{14}C$ values since the 1880s indicate a greater influx of younger surface waters, and this reduced oceanic "reservoir effect" overrides the anticipated Suess effect (Fig. 3F). We interpret this shift as a weakening of the wind-driven SEC since the late 19th century, which reduced the transport of upwelled equatorial ^{14}C-depleted water to the GBR corals.

Our SSTA reconstructions suggest that a stronger latitudinal temperature gradient, relative to the present, may have prevailed during the LIA. General circulation model experiments (*9*) indicate that the global climate responds to an exaggerated latitudinal temperature difference by intensifying the large-scale atmospheric dynamics of the Hadley circulation cells in order to maintain thermal balance. During the LIA, if warm tropical Pacific SSTs encouraged evaporation (as implied by the coral $\delta^{18}O$ records) and a stronger Hadley circulation dried the subtropics, then global average water vapor should have increased. A critical question is where that moisture was transported. Generally, snow cover increases with a strong latitudinal temperature gradient, in part because of cooler high-latitude conditions, but also as a result of a greater atmospheric connection between the tropics and extratropics (*10*). Our results imply that the tropical oceans may have played an important role in driving the LIA glacial expansion during the repeated advances between 1600 and 1860 (*1*). Cooling and abrupt freshening of the tropical southwestern Pacific coincided with the weakening of atmospheric circulation at the end of the LIA, when glaciers worldwide began to retreat.

References and Notes

1. J. M. Grove, *The Little Ice Age* (Methuen, London, 1988).
2. T. J. Crowley, G. R. North, *Paleoclimatology* (Oxford Univ. Press, New York, 1991).
3. H. H. Lamb, *Climate, History and the Modern World* (Routledge, London, ed. 2, 1995).
4. R. S. Bradley, P. D. Jones, *The Holocene* **3**, 367 (1993).
5. K. J. Kreutz *et al.*, *Science* **277**, 1294 (1997).
6. L. G. Thompson, E. Mosley-Thompson, W. Dansgaard, P. M. Grootes, *Science* **234**, 361 (1986).
7. P. D. Jones, K. R. Briffa, T. P. Barnett, S. F. B. Tett, *The Holocene* **8**, 455 (1998).
8. P. D. Jones, T. J. Osborn, K. R. Briffa, *Science* **292**, 662 (2001).
9. D. Rind, *J. Geophys. Res.* **103**, 5943 (1998).
10. ———, *Quat. Sci. Rev.* **19**, 381 (2000).
11. See supplemental material on *Science* Online at www.sciencemag.org/cgi/content/full/295/5559/1511/DC1.
12. M. T. McCulloch, M. K. Gagan, G. E. Mortimer, A. R. Chivas, P. J. Isdale, *Geochim. Cosmochim. Acta* **58**, 2747 (1994).
13. M. K. Gagan *et al.*, *Science* **279**, 1014 (1998).
14. E. J. Hendy, M. K. Gagan, J. M. Lough, in preparation.
15. Sr/Ca and U/Ca were determined by isotope dilution and analyzed by thermal ionization mass spectrometry and solution inductively coupled plasma mass spectrometry, respectively. For methodological details, see (*11*).
16. The composite reconstructions are the average of all records, after normalization relative to the longest continuous record (HAV-01B). The $\delta^{18}O$ composite is based on eight cores; the Sr/Ca and U/Ca composites are constructed from seven (PAN08B excluded). Error bounds were calculated using 95% confidence intervals for each 5-year period. Periods of higher U/Ca variability coincide with die-offs in two of the cores in 1782–1785 and 1817. Data are available at www.ngdr.noaa.gov/paleo/pubs/hendy2002.
17. C. Alibert, M. T. McCulloch, *Paleoceanography* **12**, 345 (1997).
18. G. R. Min *et al.*, *Geochim. Cosmochim. Acta* **59**, 2025 (1995).
19. N. A. Rayner, E. B. Horton, D. E. Parker, C. K. Folland, K. B. Hackett, *Version 2.2 of the Global Sea–Ice and Sea Surface Temperature Data Set, 1903–1994* (Hadley Centre for Climate Prediction and Research, Meteorological Office, Bracknell, Berkshire, UK, 1996).
20. M. Bottomley, C. K. Folland, J. Hsiung, R. E. Newell, D. E. Parker, *Global Ocean Surface Temperature Atlas "GOSTA"* (U.K. Meterological Office, Her Majesty's Stationary Office, London, 1990).
21. B. K. Linsley, G. M. Wellington, D. P. Schrag, *Science* **290**, 1145 (2000).
22. K. R. Briffa, P. D. Jones, F. H. Schweingruber, T. J. Osborn, *Nature* **393**, 450 (1998).
23. M. E. Mann, R. S. Bradley, M. K. Hughes, *Nature* **392**, 779 (1998).
24. T. J. Crowley, *Science* **289**, 270 (2000).
25. P. K. Swart, M. L. Coleman, *Nature* **283**, 557 (1980).
26. The $\delta^{18}O$ residual is calculated as

$$\Delta\delta^{18}O = \partial\delta^{18}O/\partial T(T_{\delta^{18}O} - T_{Sr/Ca})$$

where the temperature-dependent function, $\partial\delta^{18}O/\partial T$, is −0.18/°C for *Porites* sp. (*13*).
27. E. R. M. Druffel, S. Griffin, *J. Geophys. Res.* **98**, 20 (1993).
28. T. M. Quinn *et al.*, *Paleoceanography* **13**, 412 (1998).
29. T. M. Quinn, F. W. Taylor, T. J. Crowley, *Quat. Sci. Rev.* **12**, 407 (1993).
30. M. N. Evans, A. Kaplan, M. A. Cane, *Paleoceanography* **15**, 551 (2000).
31. T. J. Crowley, T. M. Quinn, W. T. Hyde, *Paleoceanography* **14**, 605 (1999).
32. B. K. Linsley, R. B. Dunbar, G. M. Wellington, D. A. Mucciarone, *J. Geophys. Res.* **99**, 9977 (1994).
33. E. Wolanski, *Physical Oceanographic Processes of the Great Barrier Reef* (CRC Press, Boca Raton, FL, 1994).
34. J. M. Lough, *Int. J. Clim.* **17**, 55 (1997).
35. P. J. Isdale, B. J. Stewart, K. S. Tickle, J. M. Lough, *The Holocene* **8**, 1 (1998).
36. T. Delcroix, C. Henin, V. Porte, P. Arkin, *Deep-Sea Res.* **43**, 1123 (1996).
37. S. Sokolov, S. Rintoul, *J. Mar. Res.* **58**, 223 (2000).
38. E. R. M. Druffel, S. Griffin, *J. Geophys. Res.* **104**, 23607 (1999).
39. M. Stuiver, G. W. Pearson, T. F. Braziunas, *Radiocarbon* **28**, 980 (1986).

40. We thank L. Kinsley, H. Scott-Gagan, and J. Cali for analytical assistance; S. Fallon and G. Mortimer for the U/Ca method development; B. Parker and M. Devereux for assistance with the corals; and J. Chappell, C. Hendy, G. Meyers, and two anonymous reviewers for valuable comments on the manuscript. E.J.H. was supported by an Australian Postgraduate Award.

2 November 2001; accepted 22 January 2002

Microbial Activity at Gigapascal Pressures

Anurag Sharma,* James H. Scott,* George D. Cody, Marilyn L. Fogel, Robert M. Hazen, Russell J. Hemley, Wesley T. Huntress

We observed physiological and metabolic activity of *Shewanella oneidensis* strain MR1 and *Escherichia coli* strain MG1655 at pressures of 68 to 1680 megapascals (MPa) in diamond anvil cells. We measured biological formate oxidation at high pressures (68 to 1060 MPa). At pressures of 1200 to 1600 MPa, living bacteria resided in fluid inclusions in ice-VI crystals and continued to be viable upon subsequent release to ambient pressures (0.1 MPa). Evidence of microbial viability and activity at these extreme pressures expands by an order of magnitude the range of conditions representing the habitable zone in the solar system.

Microbial communities adapt to a wide range of pressures, temperatures, salinities, pH, and oxidation states. Although the chemical and physical conditions in these extreme environments are reasonably well constrained, the consequence of these physical parameters on the physiology of microbial communities is not well understood. Significant attention has been focused on the effects of high and low temperature on physiology (*1, 2*). There is some evidence that elevated pressure may also manifest interesting effects on cellular physiology (*3, 4*). For example, recent studies report that elevated pressure may lead to enzyme inactivation, compromise cell-membrane integrity, and suppress protein interactions with various substrates (*3–6*). Whereas the cumulative impact of these pressure-induced effects on microbial metabolism and physiology is an inhibition in growth rate and cellular division in microorganisms (*7–9*), exactly how these factors affect intact cells is not well understood (*4, 10*).

Numerous high-pressure studies have been conducted on biological systems; however, these have been either on individual biomol-

Geophysical Laboratory, Carnegie Institution of Washington, 5251 Broad Branch Road, N.W., Washington, DC 20015, USA.

*To whom correspondence should be addressed. E-mail: sharma@gl.ciw.edu (A.S.); j.scott@gl.ciw.edu (J.H.S.)